Drivers of i-DNA Formation in a Variety of Environments Revealed by Four-Dimensional UV Melting and Annealing

Mingpan Cheng, Jielin Chen, Huangxian Ju, Jun Zhou, Jean-Louis Mergny

Drivers of i-DNA formation in a variety of environments revealed by four-dimensional UV melting and annealing

Mingpan Cheng[†,‡,*], Jielin Chen[†], Huangxian Ju[†], Jun Zhou[†,*], and Jean-Louis Mergny[†,‡,§,*]

[†] State Key Laboratory of Analytical Chemistry for Life Science, School of Chemistry & Chemical Engineering, Nanjing University, Nanjing 210023, China.

[‡] ARNA Laboratory, Université de Bordeaux, INSERM U1212, CNRS UMR5320, IECB, Pessac 33607, France.

[§] Laboratoire d'Optique et Biosciences, Ecole Polytechnique, CNRS, INSERM, Institut Polytechnique de Paris, 91128 Palaiseau cedex, France.

ABSTRACT

i-DNA is a four-stranded, pH-sensitive structure formed by cytosine-rich DNA sequences. Previous reports have addressed the conditions for formation of this motif in DNA *in vitro* and validated its existence in human cells. Unfortunately, these *in vitro* studies have often been performed under different experimental conditions, making comparisons difficult. To overcome this, we developed a four-dimensional UV melting and annealing (4DUVMA) approach to analyze i-DNA formation under a variety of conditions (*e.g*., pH, temperature, salt, crowding). Analysis of 25 sequences provided a global understanding of i-DNA formation under disparate conditions, which should ultimately allow the design of accurate prediction tools. For example, we found reliable linear correlations between the mid-point of pH transition and temperature (-0.04 ± 0.003 pH unit per 1.0 °C temperature increment) and between the melting temperature and pH (-23.8 ± 1.1 °C per pH unit increment). In addition, by analyzing the hysteresis between denaturing and renaturing profiles in both pH and thermal transitions, we found that loop length, nature of the C-tracts, pH, temperature, and crowding agents all play roles in i-DNA folding kinetics. Interestingly, our data indicate which conformer is more favorable for the sequences with an odd number of cytosine base pairs. Then the thermal and pH stabilities of "native" i-DNAs from human promoter genes were measured under near physiological conditions (pH 7.0, 37 °C). The 4DUVMA method can become a universal resource to analysis the properties of any i-DNA-prone sequence.

INTRODUCTION

DNA is prone to structural polymorphism: in addition to the canonical Watson-Crick double-helix, a number of alternative structures are known. Among these oddities is the four-stranded, C-rich i-DNA structure [1-2], which forms under mildly acidic conditions that stabilize hemi-protonated $C{\cdot}C^+$ base pairs (**Figure 1A**) [3-4]. In the i-DNA structure, two interlocked parallel-stranded duplexes consisting of $C{\cdot}C^+$ base pairs are held together in a head-to-tail orientation. A typical intramolecular i-DNA involves four contiguous cytosine tracts and three loops (**Figure 1B**) [5-8]. As cytosine protonation at the N3 position is essential for formation of the hemi-protonated base pairs, stability and unfolding/folding rates of i-DNA depend on pH [9-20]. i-DNA stability is often modest under physiological conditions [11, 13, 21], but some i-DNA structures have been shown to remain folded at neutral pH [11, 13-16, 20-26]. In-cell NMR [20, 27] and experiments with an i-DNA-specific antibody [28] recently demonstrated that i-DNAs are present in human cells.

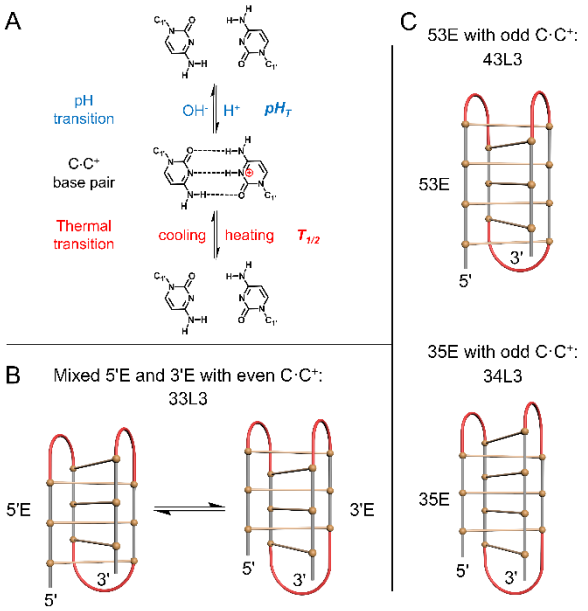

Figure 1 i-DNA formation. (**A**) Equilibrium between unpaired bases and $C{\cdot}C^+$ base pair, which are probed by determination of mid-points of pH-induced and thermal transitions, pH_T and $T_{1/2}$, respectively. (**B**) Mixed 5'E and 3'E conformers formed by the sequences with even numbers of $C{\cdot}C^+$ base pairs. Loop regions are in red. (**C**) 53E (upper) and 35E (lower) conformers formed by the sequences with odd numbers of $C{\cdot}C^+$ base pairs. Sequences of 33L3, 43L3, and 34L3 are listed in **Table 1**.

In contrast to G-quadruplexes formed by G-rich sequences, i-DNA strand orientations are fixed. Adjacent strands are always antiparallel to each other, and diagonally opposed strands run in the same direction. As a consequence, i-DNA structures are less polymorphic than G-quadruplexes. Nevertheless, some variability is observed in i-DNA structures: For sequences with an even number of $C{\cdot}C^+$ base pairs, two conformers, called 5'E and 3'E, are possible, as the two external solvent accessible $C{\cdot}C^+$ base pairs may be located at either the 5' or the 3' ends of both duplexes, respectively (**Figure 1B**) [7-8, 29-34]. For sequences with an odd number of $C{\cdot}C^+$ base pairs, one duplex has more base pairs than the other and both 5' and 3' terminal base pairs are oriented to maximize stacking interactions [12, 19, 35-37]. Two different arrangements are observed depending on primary sequence (**Figure 1C**): In the 53E arrangement (not to be confused with 5'E), the (n+1) C-tracts are the first and third runs of cytosines. In the 35E conformer, the (n+1) C-tracts at the second and fourth positions. For example, sequences 43L3 [d($C_4T_3C_3T_3C_4T_3C_3$)] and 34L3 [d($C_3T_3C_4T_3C_3T_3C_4$)] adopt 53E and 35E folds, respectively.

i-DNA stability depends on the number of $C{\cdot}C^+$ base pairs, and structures with longer central loops are more stable than those with shorter loops [11, 13, 20, 24]. In addition to pH and temperature, cation type and concentration influence both stability and conformation: Na^+, K^+, Li^+, NH_4^+, and Cu^{2+} destabilize i-DNA [5, 38-40], whereas Ag^+ and Cu^+ stabilize this structure [41-44]. Moreover, i-DNA has been reported to be stabilized by macromolecular crowding conditions [45-50].

Mid-points of acid-alkaline (pH) and thermal transitions, referred to here as pH_T and $T_{1/2}$, respectively, are often used to determine the stability of i-DNAs (**Figure 1A**). However, comparing results is often difficult as pH_T is often determined at a given temperature, and thermal stability is only measured at a few pH values [5, 11, 13-16, 20]. These limited measurements do not provide a reliable global picture of pH_T dependency on temperature or of thermal stability on pH and do not allow the determination of the folded fraction under a range of conditions. To illustrate the need for standardization, in two recent papers [11, 13], the melting temperature of i-DNA formed by the same sequence, $d(C_4T_3C_4T_3C_4T_3C_4)$, was found to be 71.7 °C and 56.4 °C; the values were measured at pH 5.0 with 37 mM K^+ and pH 5.5 with 110 mM Na^+, respectively. The pH_T values also differed: Values were 6.95 and 7.1, measured at 23 °C and 20 °C, respectively.

In order to overcome these limitations, we developed a systematic four-dimensional analysis of UV melting and annealing (4DUVMA). The 4DUVMA approach measures the UV absorbance spectra (220-330 nm wavelength range) over the pH range between 5.0 and 8.0 at temperature range between 5 to 90 °C. In contrast with recent studies in which we analyzed over 200 sequences in a limited set of conditions [20, 24], here we evaluated a smaller panel of 20 sequences with 6 to 12 $C{\cdot}C^+$ base pairs (**Table 1**) in far more conditions. Formation diagrams were constructed for each i-DNA in which the fraction folded was determined under all pH and temperature combinations. This analysis allowed us to establish clear correlations between pH_T and temperature and between $T_{1/2}$ and pH. Furthermore, we found that conformer 53E is more stable than 35E for all sequences with an odd $C{\cdot}C^+$ base pair number. We then applied the 4DUVMA method to five sequences with the potential to form i-DNA found in human promoter regions. Finally, the effect of molecular crowding on i-DNA stability and hysteresis was investigated.

RESULTS

Here we systematically analyzed 20 model sequences (**Table 1**) using 4DUVMA. The C-tracts of these sequences range in length from three to six, allowing the formation of up to 12 $C{\cdot}C^+$ base pairs, thus avoiding complex biphasic melting profiles observed for longer sequences [11, 13]. The total number of nucleotides involved in loops, defined as *loop size*, is either three or nine nucleotides. Sequences are named based on the lengths of C-tracts and individual loops.

Table 1 Twenty model sequences used in this work.

Name	Sequence (5'→3')	$C{\cdot}C^+$ no. [a]	loop size [b]	nt [c]	Conformation [d]	Molecularity [e]
33L1	CCCTCCCTCCCTCCC	6	3	15	mix	dm
33L3	CCCTTTCCCTTTCCCTTTCCC	6	9	21	mix	m
34L1	CCCTCCCCTCCCTCCCC	7	3	17	35E	dm
34L3	CCCTTTCCCCTTTCCCTTTCCCC	7	9	23	35E	m
43L1	CCCCTCCCTCCCCTCCC	7	3	17	53E	m(d)
43L3	CCCCTTTCCCTTTCCCCTTTCCC	7	9	23	53E	m
44L1	CCCCTCCCCTCCCCTCCCC	8	3	19	mix	m(d)
44L3	CCCCTTTCCCCTTTCCCCTTTCCCC	8	9	25	mix	m
45L1	CCCCTCCCCCTCCCCTCCCCC	9	3	21	35E	m
45L3	CCCCTTTCCCCCTTTCCCCTTTCCCCC	9	9	27	35E	m
54L1	CCCCCTCCCCTCCCCCTCCCC	9	3	21	53E	m
54L3	CCCCCTTTCCCCTTTCCCCCTTTCCCC	9	9	27	53E	m
55L1	CCCCCTCCCCCTCCCCCTCCCCC	10	3	23	mix	m
55L3	CCCCCTTTCCCCCTTTCCCCCTTTCCCCC	10	9	29	mix	m
56L1	CCCCCTCCCCCCTCCCCCTCCCCCC	11	3	25	35E	m
56L3	CCCCCTTTCCCCCCTTTCCCCCTTTCCCCCC	11	9	31	35E	m
65L1	CCCCCCTCCCCCTCCCCCCTCCCCC	11	3	25	53E	m
65L3	CCCCCCTTTCCCCCTTTCCCCCCTTTCCCCC	11	9	31	53E	m
66L1	CCCCCCTCCCCCCTCCCCCCTCCCCCC	12	3	27	mix	m
66L3	CCCCCCTTTCCCCCCTTTCCCCCCTTTCCCCCC	12	9	33	mix	m

[a] Maximum theoretical number of $C{\cdot}C^+$ base pairs formed assuming intramolecular folding and no cytosines involved in loop formation. [b] Total number of nucleotides in the three loops assuming no cytosines are involved in loop formation. [c] Oligonucleotide total length in nucleotides. [d] Conformation: 'mix' refers to a mixture of 3'E and 5'E conformers, see text and **Figure 1** for details. [e] Molecularity was determined by SE-HPLC at pH 6.0; 'dm' indicates a mixture of dimer (major) and monomer (minor), 'm(d)' indicates a monomer with traces of a dimer, 'm' refers to a purely monomeric species.

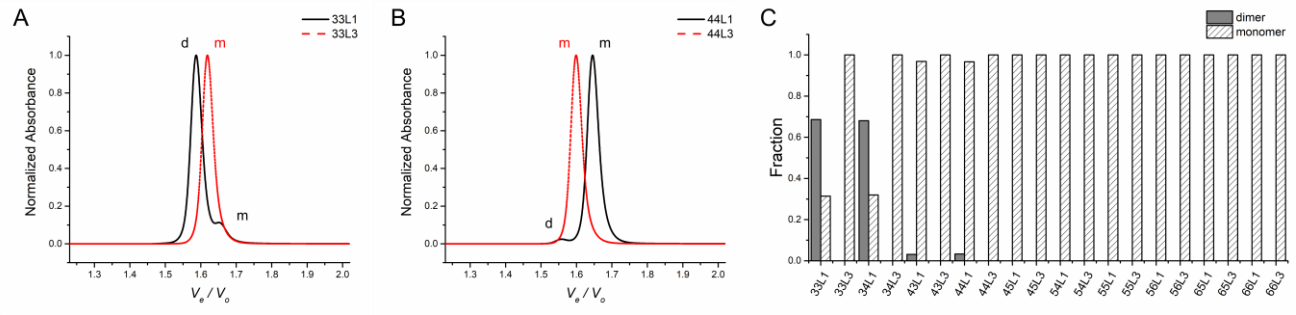

Figure 2 Molecularity of the folded species deduced from SE-HPLC analysis at pH 6.0. Normalized chromatograms of (**A**) 33L1 and 33L3 and (**B**) 44L1 and 44L3. Peaks corresponding to monomer and dimer species are marked with 'm' and 'd', respectively. (**C**) Fraction of monomeric and dimeric species for each i-DNA oligonucleotide analyzed.

Size-exclusion high performance liquid chromatography (SE-HPLC) is a powerful tool to discriminate aggregation states of quadruplex DNAs [51-52]. We used SE-HPLC to evaluate monomer to dimer ratios of the i-DNAs. Chromatography profiles of sequences at pH 6.0 are provided in **Figures 2A-B** and **Figure S1**. The so-called *structure index* [51] can be used to discriminate the

molecularity of i-DNAs; the monomer and dimer species have structure indexes around 5.8 and 6.2, respectively. The fractions of monomeric and dimeric species in each i-DNA were determined (**Figure 2C** and **Table 1**). 33L1 and 34L1 mainly fold into intermolecular i-DNAs (~68% dimer for both). 43L1 and 44L1 mainly fold into intramolecular structures (~97% monomeric for both). All other sequences exclusively (>99%) adopt an intramolecular fold.

4DUVMA experiments were then performed for each sequence. To illustrate the procedure, the temperature dependent UV spectra at pH 6.0 of 44L1 are shown in **Figures 3A-B**. The temperature-dependent thermal difference spectra (TDS) [24] were obtained by subtracting the UV spectrum of fully unfolded species at the highest temperature (90 °C) from the spectra of fully or partially folded species at a lower temperature, between 5 and 90 °C (**Figures 3C-D**). The TDS positive peak around 240 nm and negative peak around 295 nm indicate the formation of i-DNA [53]. Upon heating, the intensities of both peaks decrease, as a result of i-DNA dissociation; upon cooling, the intensities increase as i-DNA refolds. To verify the robustness of our analysis, we determined the folded fractions and the temperatures at which half of the molecules are folded ($T_{1/2}$) at different wavelengths (*e.g.*, 295, 260, 240 nm). **Figure 3F** indicates that these profiles are nearly superimposable. We chose the absorbance at 295 nm to process the data as changes at this wavelength are proportionally higher than at other wavelengths.

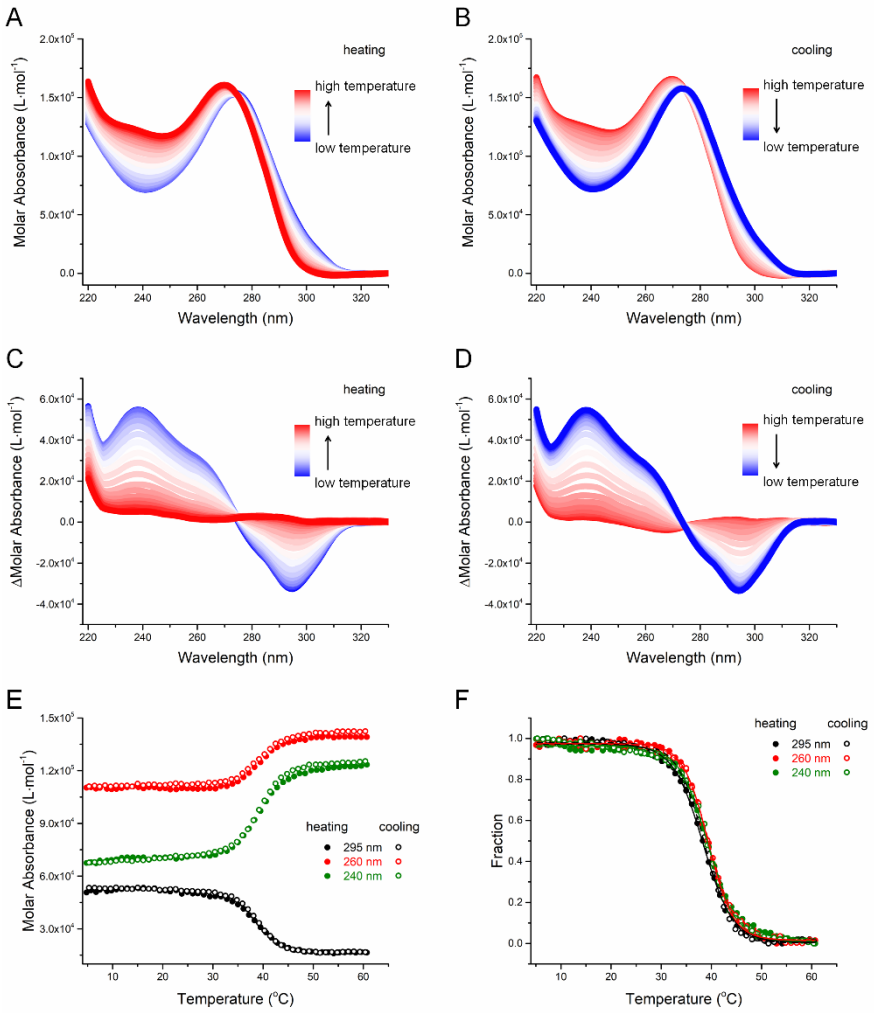

Figure 3 UV absorbance analysis of the denaturation and refolding of 44L1 at pH 6.0. Temperature dependence of the UV absorbance during (**A**) melting and (**B**) annealing in the 220-330 nm wavelength range. TDS monitored during (**C**) melting and (**D**) annealing. (**E**) Molar absorbance and (**F**) fraction folded monitored at 240, 260, and 295 nm during melting and annealing.

Denaturation and renaturation profiles for each model oligonucleotide were determined at 26 different pH values ranging from 5.0 to 8.0. These plots for the heating and cooling processes are shown for 44L1 in **Figure 4A**. As expected, stability clearly increased when pH decreased. We then determined the fraction folded at each temperature for each melting profile at a given pH, allowing us to draw the formation diagram for 44L1, shown in **Figure 4B**. Data for all other oligonucleotides are presented in **Figure S2.** From the formation diagrams, we extracted pH-dependent $T_{1/2}$ values and temperature-dependent pH_T values during both heating and cooling processes.

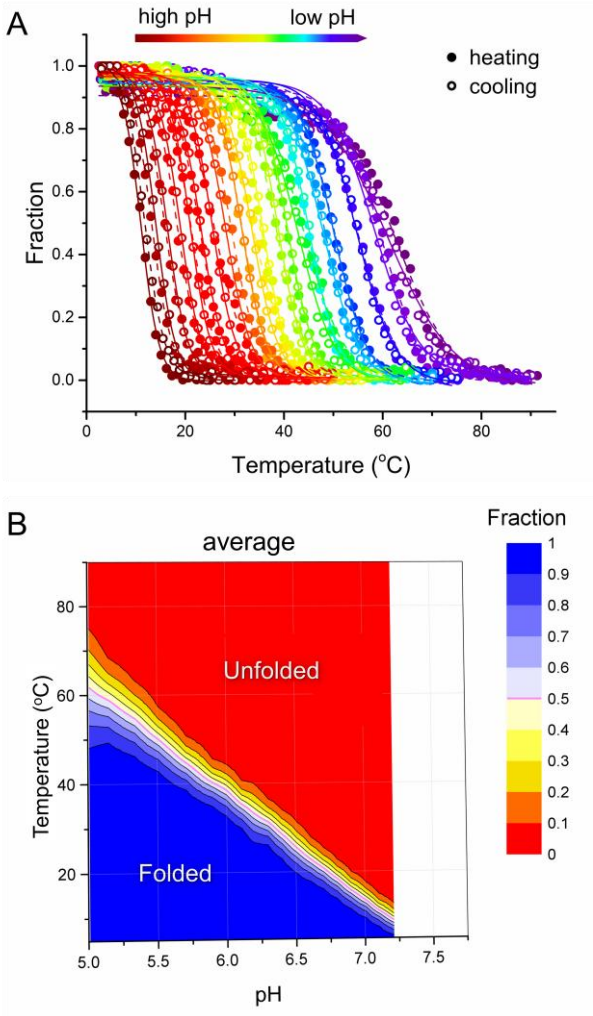

Figure 4 pH and temperature dependency of i-DNA formation for the 44L1 sequence. (**A**) Fraction folded as a function of temperature deduced from UV melting and annealing profiles at different pHs. Note that the transition is more abrupt (*i.e.*, occurs over a small temperature range) at high pHs. Nonlinear regression analysis using a two-state transition model of each individual curve is presented in supplementary information. (**B**) Formation diagram of i-DNA under different pH and temperature combinations. The fraction here corresponds to the average of two determinations made during the melting and annealing processes. Note that the region corresponding to partial formation, in yellow, is smaller above pH 5.5, as a result of sharper (more "cooperative") transitions (panel A).

pH-dependent $T_{1/2}$ values are plotted versus pH for 44L1 in **Figure 5A**. Data for all other oligonucleotides are shown in **Figure S3**, and raw values are provided in **Table S1**. T_m in this work is defined as the average of $T_{1/2}$ obtained from heating and cooling processes [10, 54]. An excellent negative linear correlation (Pearson's r > 0.99) between T_m and pH was found for all sequences in this pH range (**Figure 5B**). Linear fitting results of T_m as a function of pH are given in **Table S2**. These experiments allowed a precise and general quantitative assessment of pH dependency of i-DNA stability: T_m drops by 23.8 ± 1.1 °C per pH unit increment (**Figure 5C**); in a remarkable way, this value is nearly independent on sequence, as shown by the nearly-parallel lines in **Figure 5B**. How $C{\cdot}C^+$ base pair number and loop size affect the T_m in environments that range from acid to alkaline are depicted in **Figure 5B**: Thermal stability increased with the number of $C{\cdot}C^+$ base pairs,

and structures with longer loops were more stable than those with three single-nucleotide loops. T_m increased monotonically with C-tract length, but this increase leveled off for long runs, as the T_m increases due to each additional C·C$^+$ base pair dropped from *ca.* 4.5 °C for the shortest to 1.5 °C for the longest oligonucleotides (**Figure 5D**). There is a difference between the two families of sequences having a total loops size of 3 or 9 nucleotides: 33L1 and 34L1 are partially or mainly folded into *intermolecular* i-DNAs, while all sequences with loop size 9 adopt *intramolecular* structures. (**Figure 2**).

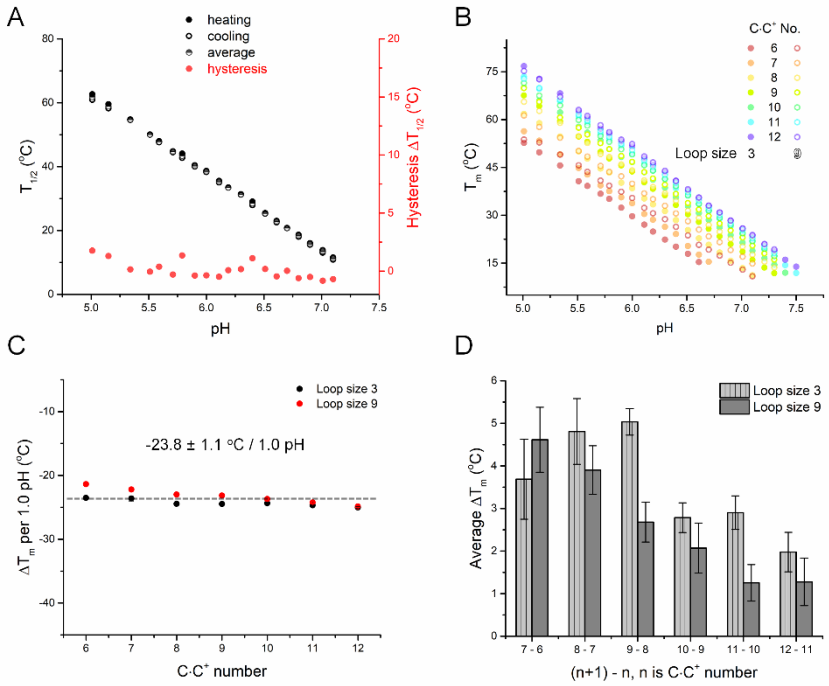

Figure 5 Thermal stability of i-DNA is pH dependent. (**A**) $T_{1/2}$ values versus pH for the 44L1 sequence. (**B**) Effects of C·C$^+$ base pair number, loop size, and pH on T_m. For the sequences with an odd number of C·C$^+$ base pairs (7, 9, or 11), T_m values are averages of two i-motifs with 53E and 35E conformers. (**C**) T_m change per pH unit increase for model sequences. (**D**) Average T_m change per each additional C·C$^+$ base pair.

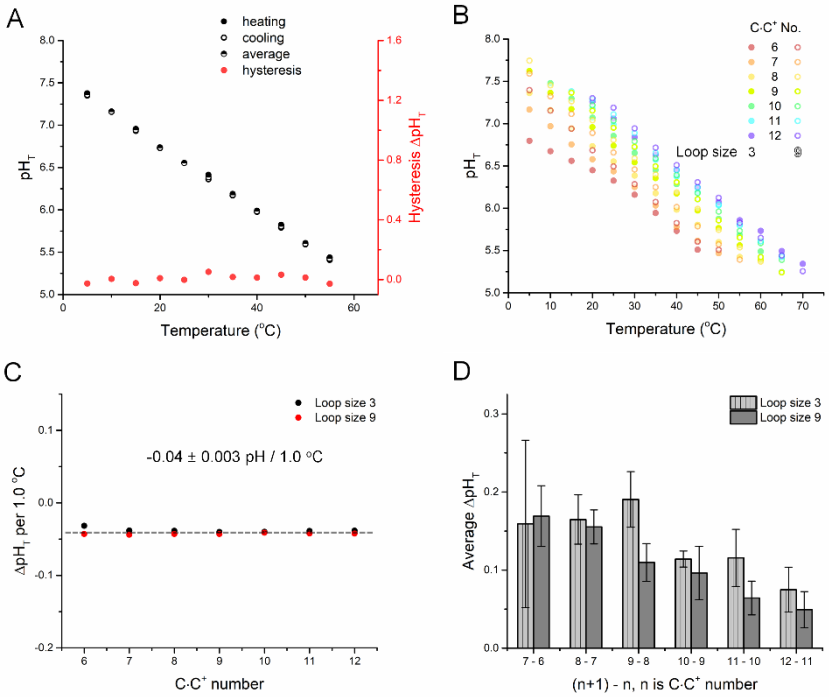

Figure 6 Temperature-dependence of pH-induced transitions of i-DNA structures. (**A**) pH_T values determined at different temperatures for 44L1. For this sequence, there is little or no hysteresis between the heating and cooling processes. (**B**) Effects of C·C$^+$ base pair number, loop size, and temperature on pH_T. For the sequences with an odd number of C·C$^+$

base pairs (7, 9, and 11), pH_T values are averages of the two i-motifs with 53E and 35E conformations. (**C**) Average pH_T change per 1.0 °C increment in temperature. (**D**) Average pH_T change per each additional C·C$^+$ base pair.

The temperature-dependence of pH_T values are presented in **Figure 6A** for 44L1. Individual curves for each sequence are given in **Figure S4**, and raw values are given in **Table S3**. An excellent negative linear correlation (Pearson's r > 0.99) between pH_T and temperature were found for all sequences (**Figure 6B**). Again, this behavior is remarkable, as all sequences exhibit similar temperature dependencies. Linear fitting results of pH_T as a function of temperature are given in **Table S2**: pH_T changed by -0.04 ± 0.003 pH unit for each 1.0 °C temperature increment (**Figure 6C**).

While the dependency of pH_T on temperature was nearly sequence-independent, pH_T values at a given temperature depended on sequence: pH_T increased with the number of C·C$^+$ base pairs, and sequences with longer loops were more stable than those with short loops. pH_T increased monotonically with C-tract length, but, as with $T_{1/2}$, this growth plateaued for long C-runs, with an increase of 0.05 pH unit per additional base pair for the longer motifs (**Figure 6D**).

Hysteresis between denaturing and renaturing processes was found for some, but not all, i-DNAs under specific conditions for both thermal and pH transitions. Transitions for 66L1 and 66L3 are presented in **Figures 7A** and **7B** as examples. Several factors influence the degree of hysteresis (**Figures 7C** and **7D**): In measurement of $T_{1/2}$, hysteresis becomes larger at higher pH; in measurement of pH_T, hysteresis becomes smaller at high temperatures. Additionally, sequences with longer loops or more C·C$^+$ base pairs had larger hysteresis for both $T_{1/2}$ and pH_T. Finally, sequences that adopt intermolecular i-DNA structures, such as 33L1 and 34L1, had larger hysteresis (for both $T_{1/2}$ and pH_T) than sequences that exclusively fold into intramolecular structures. We infer from these data that longer sequence motifs, higher pHs, and lower temperatures increase hysteresis.

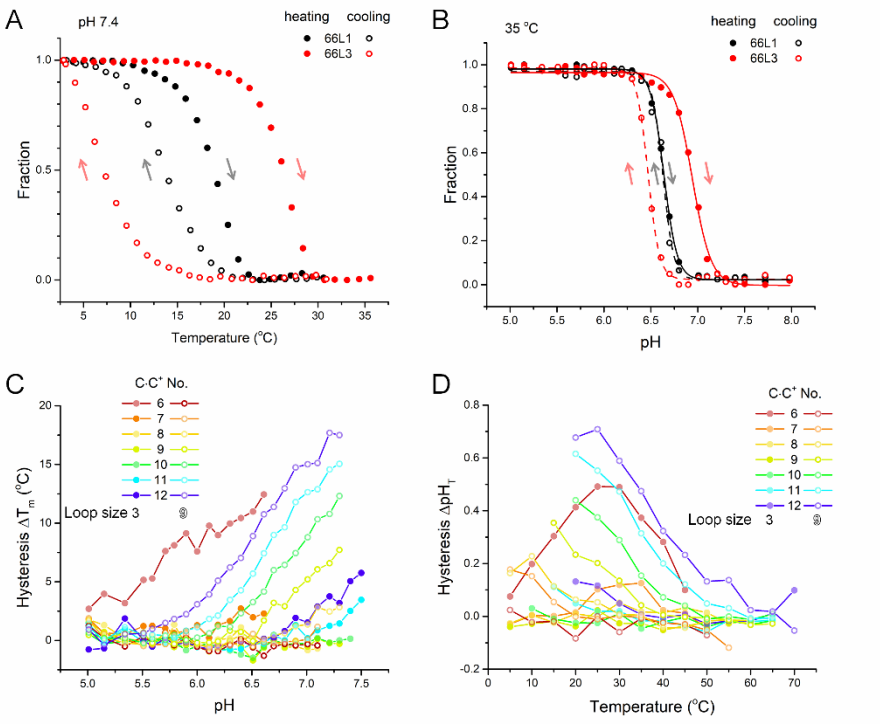

Figure 7 Hysteresis in thermal and pH transitions. Fraction folded as a function of (**A**) temperature and (**B**) pH for heating and cooling processes of 66L1 (black) and 66L3 (red). Effects of C·C$^+$ base pair number, loop size, pH and temperature on extent of (**C**) thermal hysteresis (hysteresis $\Delta T_m = T_{1/2,\text{ heating}} - T_{1/2,\text{ cooling}}$) and (**D**) pH hysteresis (hysteresis $\Delta pH_T = pH_{T,\text{ heating}} - pH_{T,\text{ cooling}}$) between the heating and cooling processes.

We then analyzed sequences with odd numbers of C·C$^+$ base pairs and with C-tracts and loop of different lengths (**Figure 8**). A consistent trend was found: Sequences compatible with a 53E conformation, in which the first and third C-tracts are longer, are systematically more stable (both in terms of T_m and pH_T) than those with a 35E conformation in which the second and last C-tracts are longer. This observation is valid for all motifs and all experimental conditions tested here, independently of loop size (3 or 9) or total number of base pairs (7, 9 or 11) or temperature or pH (**Figures 8A-D**). The differences did tend to decrease when the number of C·C$^+$ base pairs increased: Averaged T_m differences are 4, 3, and 2 °C for 7, 9, and 11 base pairs, respectively (**Figure 8E**), and averaged pH_T differences are around 0.15, 0.10, and 0.07 pH unit for 7, 9, and 11 base pairs, respectively (**Figure 8F**).

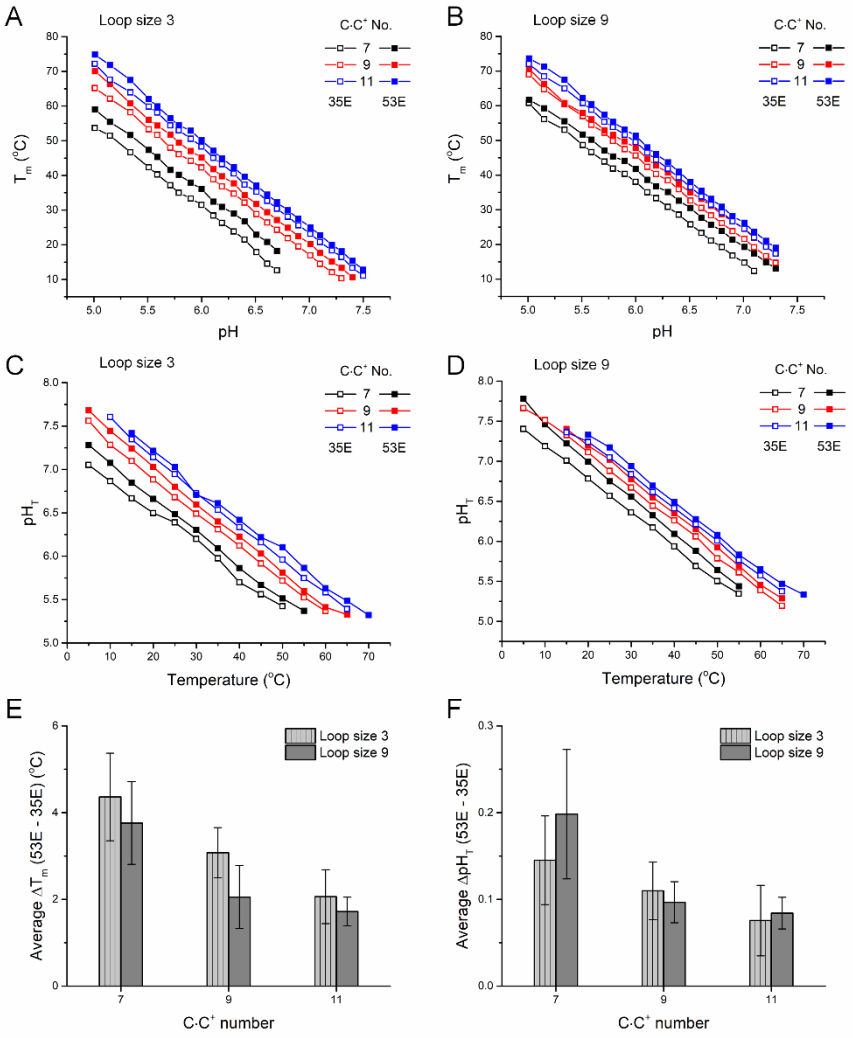

Figure 8 Thermal and pH stabilities of 35E and 53E conformations. (**A** and **B**) T_m versus pH and (**C** and **D**) pH_T versus temperature for sequences with 35E and 53E conformations. (**E**) Average difference in T_m and (**F**) average difference in pH_T of 35E and 53E conformations at different pHs as a function of number of C·C$^+$ base pairs. 34L1, 43L1, 34L3, 43L3, 45L1, 54L1, 45L3, 54L3, 56L1, 65L1, 56L3, and 65L3 were included in the analysis.

pH_T and T_m values alone do not provide a full view of the thermodynamic properties of i-DNA sequences. Therefore, we selected four sequences (33L3, 34L3, 43L3, and 44L3) that exclusively form intramolecular structures (**Figure 2**) and performed thermodynamic analyses at different pHs (**Figures S5-S8**), to determine model-dependent Gibbs free energies ($\Delta G°$) (**Figure 9A**). For an intramolecular equilibrium, K_a is equal to $\theta/(1 - \theta)$ and $\Delta G°$ is equal to 0 at the T_m ($\theta = 0.5$). Analyses

of $\Delta G°$ and K_a values of the four sequences led to several conclusions. First, formation of all i-DNAs was thermodynamically favorable ($\Delta G° < 0$) at low pH. For the sequences with 6, 7, and 8 $C{\cdot}C^+$ base pairs at pH 5.5, $\Delta G°$ values were -28, -36, and -45 $kJ{\cdot}mol^{-1}$ at 20 °C, respectively, and -9, -16, and -23 $kJ{\cdot}mol^{-1}$ at 37 °C, respectively. Second, stability decreases rapidly with pH: $\Delta G°$ became less negative or even positive at high pH, conditions under which i-DNA formation becomes thermodynamically unfavorable ($\Delta G° > 0$). For example, at pH 7.1, $\Delta G°$ values for the sequences with 6, 7, and 8 $C{\cdot}C^+$ base pairs were +14, +8, and +3 $kJ{\cdot}mol^{-1}$ at 20 °C, respectively, and +41, +32, and +30 $kJ{\cdot}mol^{-1}$ at 37 °C, respectively. An excellent positive linear correlation (Pearson's $r > 0.97$, **Table S4**) was found between $\Delta G°$ and pH for the four tested sequences. Each increase of one pH unit translated into a change in $\Delta G°$ of 27.6 ± 1.9 and 31.3 ± 1.9 kJ/mol at 20 °C and 37 °C, respectively. Third, the sequences with more $C{\cdot}C^+$ base pairs had lower $\Delta G°$ values and therefore formation of i-DNA was more thermodynamically favorable for these sequences than for those with the potential to form fewer $C{\cdot}C^+$ base pairs. Fourth, the differences in $\Delta G°$ were relatively larger at low pHs and smaller at high pHs (**Figure 9A**). Fifth, as shown in **Figure 9B**, the $\Delta G°$ of the 53E conformation is lower than that of the 35E conformation across the entire pH range, but the difference became larger at higher pHs.

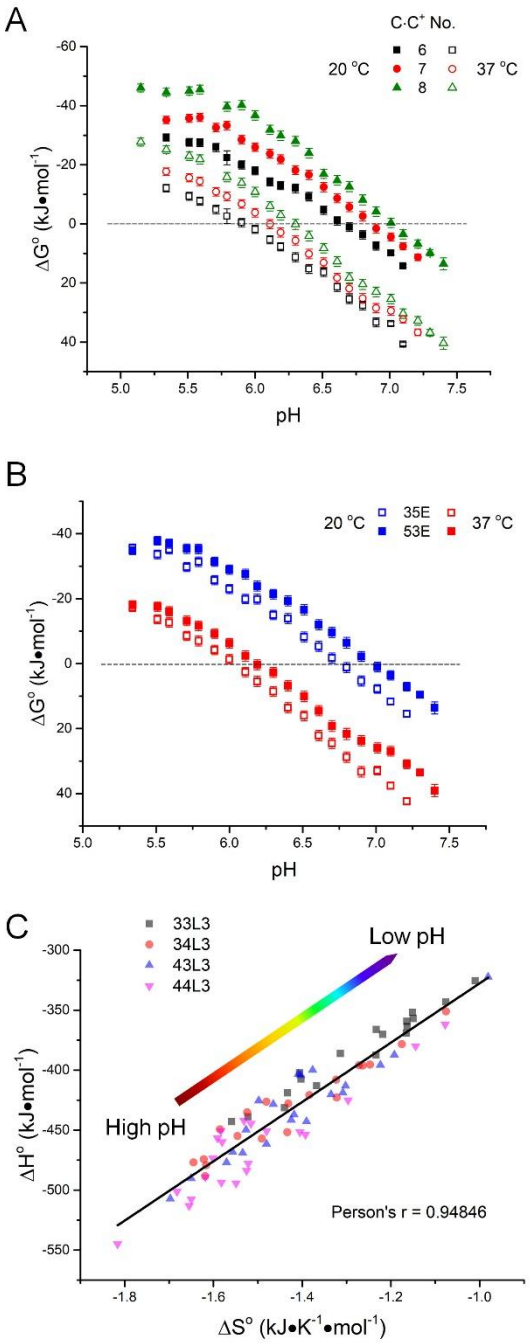

Figure 9 Thermodynamic analysis of i-DNA structures. (**A**) $\Delta G°$ versus pH for i-DNAs with 6 (33L3), 7 (average of 34L3 and 43L3), and 8 (44L3) $C{\cdot}C^+$ base pairs. (**B**) $\Delta G°$ versus pH for 35E (34L3) and 53E (43L3) conformations. (**C**) $\Delta H°$ versus $\Delta S°$ for i-DNAs with 6, 7, and 8 $C{\cdot}C^+$ base pairs in solutions over a pH range from 5.0 to 8.0 reveals a linear enthalpy-entropy compensation correlation.

Finally, even though both changes in enthalpy ($\Delta H°$) and entropy ($\Delta S°$) were generally less negative at high pH during the denaturing processes, the relative reduction in $\Delta S°$ is greater than that in $\Delta H°$, leading to an increase in $\Delta G°$ with pH. A fair linear correlation between $\Delta H°$ and $\Delta S°$ was found (**Figure 9C**), illustrative of an enthalpy-entropy compensation phenomenon. i-DNA folding is exothermic and enthalpy-driven even at neutral pH.

To better understand i-DNA properties, we investigated how parameters other than pH and temperature affect stability. Different K^+ concentrations, nature of counterions, and various molecular crowding agents were tested. These factors affect the thermal stability of i-DNA at pH 7.0 (original UV melting and annealing profiles are provided in **Figures S9** and **S10**). Interestingly, and in contrast with most other nucleic acid structures, T_m significantly *decreased* when the K^+ concentration was increased (from 17 to 10 °C for 44L1 and from 23 to 17 °C for 44L3 when K^+ concentration increased from 50 to 200 mM) (**Figure S11A**). In contrast to G-quadruplexes, the nature of the monovalent ion (K^+, Li^+, or Na^+) had little, if any, effect on T_m. For example, at pH 7.0, the T_m was 13 °C for 44L1 and 20 °C for 44L3 in the presence of each cation (**Figure S11A**).

The situation was more complex in the presence of molecular crowding agents. The T_m values increased by 6 °C for both 44L1 and 44L3 in the presence of 40 wt% PEG200 and by 10 °C in the presence of PEG8000. In contrast, Ficoll70 induced very modest changes in stability (change in T_m < 1 °C) for both sequences (**Figure S11B**).

We then investigated if one could reach the same conclusions with a different method of analysis. To this aim, we recorded the pH-dependent circular dichroism (CD) spectra (rather than UV absorbance spectra) of all 20 sequences at 20 °C (**Figure S12**). An excellent agreement was found between pH_T deduced from 4DUVMA and steady-state CD experiments (Pearson's r > 0.99), indicating that our measurements are robust and independent of the platform used.

Finally, in addition to the 20 model sequences, we also investigated the stabilities of five naturally occurring i-DNA-forming sequences (**Table 2**) from promoter regions of the following human genes [13, 22-23, 27-28, 55-56]: *DAP* (chromosome 5), *PDGF-A* (chromosome 7), *KRAS* (chromosome 12), *HIF-1α* (chromosome 12), and *BCL2* (chromosome 18). The rationale behind the study of natural sequences was to check if the conclusions reached with model sequences would apply to motifs found in genomes, which can be more complicated, with a variable number of C-tracts, different loop lengths and base compositions. CD analyses showed that all can fold into intramolecular i-DNAs (**Figure S13**), as confirmed by SE-HPLC analyses (**Figure S14**). The 4DUVMA analysis allowed to determine the pH and temperature-dependent TDS (**Figure S15**), fraction folded under different pHs and temperatures (**Figure S16**), and formation diagrams (**Figure S17**). We found that even the most stable i-DNAs under low pH conditions, such as those from *DAP* and *PDGF-A* promoters, do not form stable i-DNA under 'classical' human physiological conditions (pH 7.0 and 37 °C; **Figure S17**). However, partial formation is still observed (<50%: Tm is below 37°C). In addition, pH and temperature are heterogeneous and fluctuate in different organs, which might favor the formation of i-DNA in cells [28, 57].

Table 2 Sequences of human promoter regions with i-DNA-forming potential studied here.

Gene name	Sequence (5'→3')	nt	Reference
DAP	CCCCCGCCCCCGCCCCCGCCCCCGCCCCC	29	[13, 27]
PDGF-A	CCGCGCCCCTCCCCCGCCCCCGCCCCCGCCCCCCCCCCCC	41	[22, 27]

KRAS	GCCCGGCCCCCGCTCCTCCCCCGCCGGCCCGGCCCGGCCCCCTCCTTCTCCCCG	54	[55]
HIF-1α	CGCGCTCCCGCCCCCTCTCCCCTCCCCGCGC	31	[22, 27]
BCL2	CAGCCCCGCTCCCGCCCCCTTCCTCCCGCGCCCGCCCCT	39	[23, 28, 56]

These natural motifs obey the same rules found for model sequences: Linear correlations between T_m and pH and between pH_T and temperature were found (**Figures 10A-B**). Linear fitting results (slope, intercept, and Pearson's r) are summarized in **Table S2**. The results of individual $T_{1/2}$ and pH_T from both melting and annealing processes, and corresponding standard errors are given in **Tables S5** and **S6**. These dependencies of T_m on pH and of pH_T on temperature are generally within the range found for model sequences (**Table S2**); exceptions are the slopes in temperature transitions of i-DNAs from *KRAS* and *HIF-1α* promoters, which are -20.60 and -19.86, respectively. The guanines in these i-DNAs may participate in the formation of G:C base pairs that enhance thermal stability of the structures. formed. Hysteresis in temperature and pH transitions were positively and negatively correlated with pH and temperature, respectively (**Figures 10C-D**) as observed with model sequences. Hysteresis in the transitions of the *KRAS* i-DNA are larger than other four sequences, likely due to its longer loops.

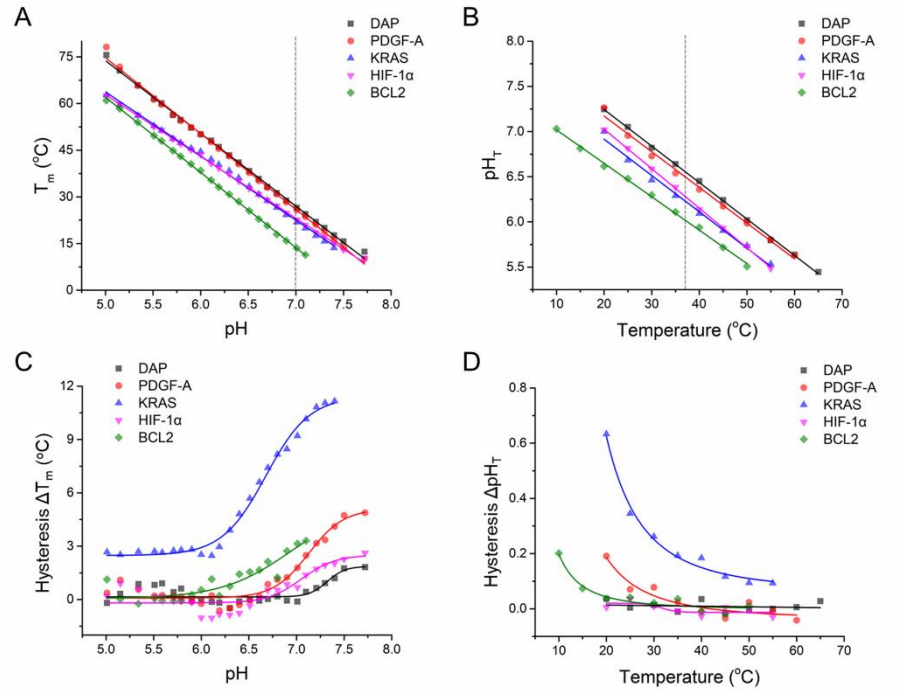

Figure 10 Thermal and pH stabilities of i-DNAs corresponding to regions of human promoters. (**A**) T_m and (**B**) averaged pH_T (vertical dotted line is centered at pH 7.0 in panel **A** and at 37 °C in panel **B**); (**C**) thermal hysteresis and (**D**) pH hysteresis.

As i-DNA stability in cells has been found to be higher than *in vitro* [20, 27], we tested thermal stability of promoter i-DNAs in the presence of crowding agents. UV-melting/annealing profiles are given in **Figure S18**. Thermodynamic parameters are summarized in **Tables S7-S8**. Thermal stability is slightly affected by Ficoll70 (-1 °C < ΔT_m < 4 °C), but greatly enhanced by PEG200, in agreement with what was observed for the model sequences (**Figures 11A** and **11B**). Interestingly, the thermal hysteresis decreased in the presence of crowding agents (**Figure 11C**), which means that the folding kinetics are faster. For example, thermal hysteresis for the *KRAS* i-DNA dropped from 9.2 °C in the absence of crowding agents to 2.7 and 2.3 °C in the presence of 40 wt% Ficoll70 and PEG200, respectively.

Generally, i-DNA formation in the presence of both crowders is less enthalpy driven ($\Delta H°$ is less negative) than in buffer (**Figure 11D**). A similar result is found for entropies ($\Delta S°$s are less negative, **Figure 11E**), whereas $\Delta G°$s are more negative at 20 °C and less positive at 37 °C (**Figures 11F** and **S19**). However, these crowding effects depend on sequence and nature of crowders (**Figure 11**, **Tables 3**, and **S7-S8**). For example, $\Delta H°$s and $\Delta S°$s became more negative for *DAP*- and *PDGF-A*-derived i-DNAs when the Ficoll70 concentration was increased from 20 to 40 wt% and for the *BCL2*-derived i-DNA when the PEG200 concentration was increased from 20 to 40 wt%. $\Delta H°$s and $\Delta S°$s for the other sequences became less negative when either Ficoll70 or PEG200 concentration was increases. Upon addition of Ficoll70, $\Delta G°$s at 20 °C decreased slightly, by -0.8 kJ•mol^{-1} to -4 kJ•mol^{-1}) which is consistent with the small changes in T_ms induced by Ficoll70. However, the $\Delta G°$s at 37 °C for i-DNAs derived from *KRAS*, *HIF-1α*, and *BCL-2* promoters were more affected, with changes ranging from -5 kJ•mol^{-1} to -11 kJ•mol^{-1} in the presence of 40 wt% Ficoll70. PEG200 induced a strong decrease in ΔG^o for all i-DNAs tested, indicating that formation of i-DNAs derived from promoter occurs under physiologically relevant (neutral pH; 37 °C) crowded conditions is thermodynamically favored (**Figure 11F** and **Table 3**).

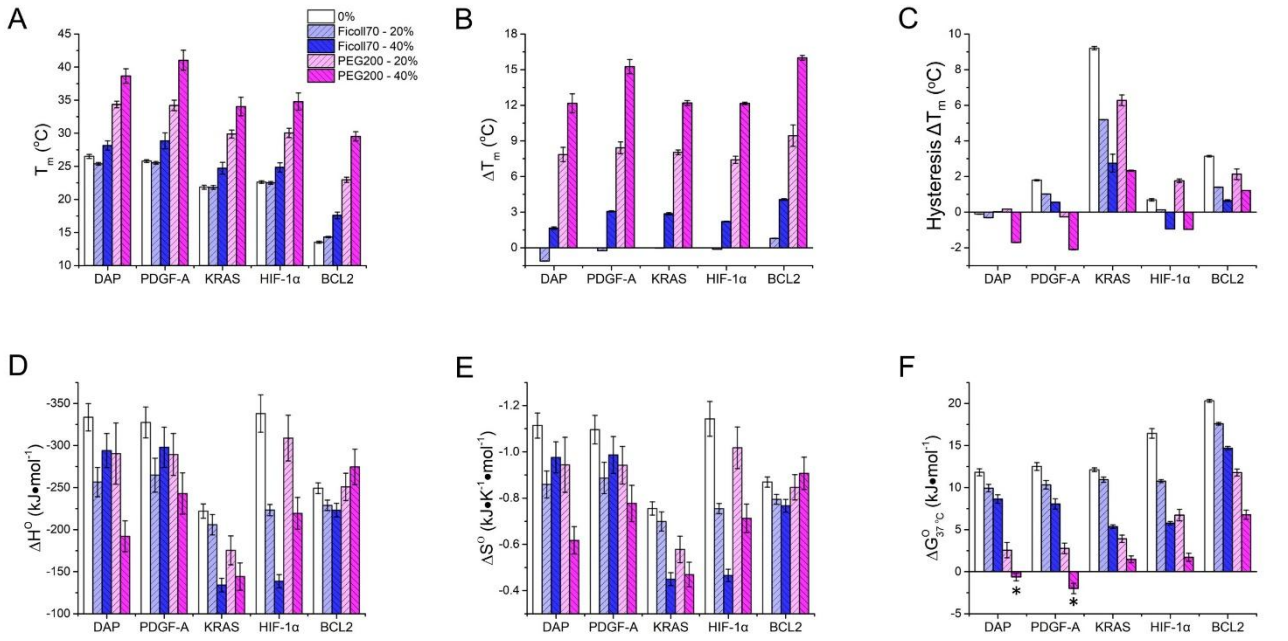

Figure 11 Thermal stability and thermodynamic of i-DNAs in human promoter genes under neutral pH (7.0) and crowding environments. The crowders added are indicated in colors of white (0 %, without crowder), light blue (20 wt% Ficoll70), blue (40 wt% Ficoll70), light red (20 wt% PEG200), and red (40 wt% PEG200). (**A**) T_m; (**B**) T_m changes induced by the crowders, where $\Delta T_m = T_{m,\text{ crowder}} - T_{m,\ 0\ \%}$; (**C**) Thermal hysteresis; (**D**) $\Delta H°$; (**E**) $\Delta S°$; (**F**) $\Delta G°$ at 37 °C (the negative $\Delta G°$ values are labeled with asterisks).

Table 3 Thermal and pH stability under near physiological condition: pH_T at 37 °C, T_m (°C) at pH 7.0, $\Delta G°$ (kJ•mol^{-1}) at pH 7.0 and 20 °C or 37 °C in the absence of and presence of 40 wt% crowding agents. [a]

Name	pH_T at 37 °C	T_m at pH 7.0			$\Delta G°$ at 20 °C and pH 7.0			$\Delta G°$ at 37 °C and pH 7.0		
		0 wt%	Ficoll70	PEG200	0 wt%	Ficoll70	PEG200	0 wt%	Ficoll70	PEG200
DAP	6.6	26.5	28.2	38.7	-7.1	-8.0	-11.1	11.8	8.6	-0.6
PDGF-A	6.5	25.8	28.8	41.0	-6.1	-8.7	-15.2	12.5	8.1	-2.0
KRAS	6.2	21.8	24.7	34.0	-0.7	-2.3	-6.5	12.1	5.4	1.5
HIF-1α	6.3	22.6	24.8	34.8	-3.0	-2.1	-10.4	16.5	5.8	1.7
BCL2	6.0	13.5	17.6	29.5	5.5	1.7	-8.7	20.3	14.7	6.8

[a] pH_Ts at 37 °C deduced from the linear fitting of pH_T as a function of temperature; $\Delta G°$s from **Table S8**.

DISCUSSION

Herein, model pyrimidine oligonucleotides were tested for their ability to form i-DNA under a range of pH and temperature conditions using our 4DUVMA strategy. The sequences with fewer $C{\cdot}C^+$ base pairs and shorter loops folded into intermolecular species, in agreement with observation by Školáková *et al.* [11], while longer sequences with runs of seven or more cytosines often exhibit dual transitions, described in previous reports [11, 13]. We therefore restricted the analysis to model sequences expected to form 6 to 12 $C{\cdot}C^+$ base pairs (*i.e.,* containing four runs of 3 to 6 cytosines). By systematically exploring effects of large temperature and pH ranges on a diverse set of sequences (25 in total), we are able to quantitatively assess the effect of pH and temperature on i-DNA stability, allowing us to draw general and quantitative rules regarding effects of sequence and conditions on i-DNA stability.

First, as expected, oligonucleotides with longer C-tracts adopted more stable i-DNA structures, as shown by lower $\Delta G°$ values and higher T_m. This increase was not linear: each additional $C{\cdot}C^+$ base pair induced an increase in T_m of 4.5 to 1.5 °C, whereas pH_T increased from *ca.* 0.15 to 0.05 pH unit. This non-linear behavior is not surprising, as DNA duplexes actually behave the same way [58-59]. A similar explanation may be proposed for both structures: one must first keep in mind that T_m is related, but not directly proportional, to $\Delta G°_{37°C}$: as the number of base pairs increases, the melting profiles become sharper and sharper, as $\Delta H°$ increases (the transition seems more "cooperative"): this means that even if the increase in T_m is smaller, the $\Delta\Delta G°$ may be similar. In addition, past a given length of helix, certain approximations such as two-state melting are no longer usable [59-60].

Second, hysteresis between the thermal denaturation and renaturation processes has been observed [5, 10-11, 13, 20, 61] and hysteresis between pH denaturation and renaturation processes has also been found [12, 61]. This is the first report in which hysteresis for *both* thermal and pH transitions is analyzed simultaneously. Both thermal and pH hystereses were more pronounced for longer sequences, at higher pHs, and at lower temperatures.

Third, and more surprising, was the systematic difference in stability between 53E and 35E motifs. At first glance, the energetic difference between 53E and 35E (or between 5'E and 3'E) should be negligible, given that an identical number of base pairs are formed with identical loops. Our results indicate that this is not the case, and examples in the literature support this conclusion. For example, the tetramolecular i-DNA formed by $[d(CCCC)]_4$ (PDB ID: 190D) is exclusively observed in a 5'E arrangement in the crystal [62], whereas $[d(CC)]_4$ (PDB ID: 1M6A) mainly adopts a 3'E conformation in solution [63-64]. Stacking interactions from proximal non-cytosine nucleobases [19, 65], unique hydrogen bonding [64, 66], and external factors including pH [8] and cation [32, 64] also affect the conformations adopted.

Fourth, an increase in pH of one unit leads to a decrease in T_m of 23.8 ± 1.1 °C in the pH range from 5.0 to 8.0. Indeed, a linear correlation of T_m on pH was previously found [5, 9]. However, these results were obtained on a limited set of sequences corresponding to i-DNAs with short C_2 or C_3 tracts. These motifs are less likely to be physiologically relevant, as their stability is marginal at physiological pH. In this work performed on a large set of sequences, this reduction of T_m varies between 19.9 °C (for *HIF-1α*) and 25.0 °C (for 66L1); it extends this conclusion to a larger pH window on physiologically relevant motifs, demonstrated to be formed in cells [20, 27]. This linear effect is only weakly dependent on the sequence (-23.8 ± 1.1 °C per pH unit). This dependency is slightly lower for the i-DNA derived from the *HIF-1α* promoter due to the potential contribution of other pairing schemes (*i.e.,* GC base pairs which are nearly pH-independent under these conditions [67]). The formation of additional Watson-Crick base pairs in i-DNA may therefore play a significant role on stability when approaching neutrality, leading to a relatively lower absolute slope of T_m versus pH.

Fifth, negative linear correlations were found between pH_T and temperature (-0.04 ± 0.003 pH unit per 1.0 °C temperature increase) for all sequences. Again, this effect, which was never quantified before, is weakly sequence-dependent (maximal and minimal values are -0.038 and -0.043 pH unit, respectively).

These linear correlations between pH_T and temperature, as well as between T_m and pH, are very useful, as they allow to predict stability at pH within a large range, including for physiologically relevant i-DNAs. An impressive finding is that these linear correlations are valid in a wide and physiologically relevant pH range, between 5.0 and 8.0. Below pH 5, the behavior is no longer linear, and a discussion of this phenomenon is presented in [5]: at pH >> p*K*a, the single strand is >99% deprotonated, and there is a net uptake of *n* protons when forming *n* C•C^+ base pairs. This protonation, which is exothermic, becomes harder and harder at higher pH, as reflected by a more and more negative $\Delta S°$. One can thus decompose the folding process into three main contributions: cytosine protonation, buffer deprotonation, and proper i-DNA formation.

Sixth, stability was negatively affected by ionic strength, as previously reported [5]. This is in contrast with most other nucleic acid structures studied so far [58].

Seventh, the effects of molecular crowding depended on the nature of the compound used to mimic crowding. Whereas PEG induced a significant increase in melting temperature, a nonionic synthetic polymer of sucrose, Ficoll, did not have a notable effect. No consensus has been reached regarding the effect of crowding on i-DNA stability [58]. Several groups have noted that PEG may not be appropriate for analysis of the effects of molecular crowding on quadruplex DNAs as its binds to nucleic acid structures [50, 68-70]. Hysteresis may also complicate the analysis, as crowding mimics such as PEG and Ficoll accelerate kinetics at neutral pH. A detailed analysis of their effects therefore requires the analysis of both melting and cooling processes. The observation that Ficoll only weakly affected i-DNA stability is in line with a previous finding that i-DNA and the corresponding unfolded single strand have similar volumes [36].

Based on the 4DUVMA approach, we now have the means to compare results obtained under a wide variety of experimental conditions, in terms of pH, temperature, cation nature and concentration, and crowding. This should facilitate the analysis of published data and allow the design of reliable tools to predict i-DNA stability under a given set of conditions. Intracellular environments are much more complex than that in tube buffer solutions. Previous work has indicated that i-DNA is slightly more stable in cells than *in vitro* [20, 27]. Our results indicate that factors such as differences in hydration or dielectric constant or interactions with proteins [56, 71-74] or small metabolites may account for this difference. The intracellular pH, temperature and salt vary from one organism to another, and conditions vary in individual cellular organelles and compartments [75-81]. In addition, the environment is dynamic and fluctuates over time [75-76]. Considering that i-motif forming sequence may exist in the genomes of many organisms and that the i-motif has potential for use in nano-devices applied in different subcellular compartments [82-84], the 4DUVMA method described here may become a universal approach to evaluate the stability of any specific i-DNA forming sequences.

CONCLUSIONS

The comprehensive 4DUVMA approach was developed to analyze the formation of i-DNA structures by 20 model sequences and 5 human promoter-derived sequences under a variety of conditions. We observed excellent linear correlations between thermal stability and pH and between pH stability and temperature, allowing us to draw general conclusions on i-DNA pH and temperature dependencies. Analysis of the data revealed differences in stability for the i-DNAs with an odd and even numbers of C·C^+ base pairs and between the 53E and 35E motifs. Crowding was found to

facilitate the formation of i-DNAs not only from a thermodynamic point of view but also by accelerating kinetics under near physiological conditions. The 4DUVMA approach will facilitate study of natural i-DNA-forming sequences and should help designing pH-sensitive nano-devices.

MATERIALS AND METHODS

Oligonucleotides and buffers

All oligonucleotides were purchased from Integrated DNA Technologies. Oligonucleotides were desalted and used without further purification. Sequence information is provided in **Tables 1** and **2**. Buffers containing 40 mM cacodylate were adjusted to the desired pH in the range of 5.0 to 8.0 range using KOH (≥99%) or HCl (37 wt. % in H_2O) at room temperature. Cacodylate buffer was chosen as its pK_a is nearly independent of temperature [53-54, 85], which is critical for the thermal analysis of pH-sensitive structures such as the i-DNA. The final potassium concentration in all buffers was adjusted to 100 mM with KCl. For the cacodylate potassium buffers with molecular crowding agents, pH was further adjusted *after* the addition of all agents. Unless otherwise stated, these cacodylate potassium buffers were used for all experiments. Samples of 1.0 μM oligonucleotide in buffer were heated at 95 °C for 5 min, then slowly (2-3 h) cooled to room temperature and stored at 4 °C. Data were processed and analyzed by software MATLAB 2020Rb (The MathWorks, Inc.) and OriginPro 2015 (OriginLab Corp.).

Size-exclusion high-performance liquid chromatography

SE-HPLC experiments were performed as previously described [51] on a Dionex UltiMate 3000 UHPLC system (Thermo Fisher Scientific) equipped with an autosampler, a Thermo Acclaim SEC-300 column (4.6 × 300 mm; 5 μm hydrophilic polymethacrylate resin spherical particles with 300 Å pore size), and a diode array detector. Unless otherwise stated, a solution containing 40 mM cacodylate buffer, pH 6, with 100 mM potassium was used as an elution buffer and to dissolve oligonucleotides. A 30-μL aliquot of oligonucleotide solution was injected onto the column (0.15 mL/min elution flow rate at 20 °C), and elution was monitored by measuring absorbance. Chromatograms were obtained by plotting the normalized absorbance at 260 nm as a function of relative elution volume V_e/V_o, where V_e is the elution volume calculated using the retention time and flow rate, and V_o is dead volume of the system. The *structure index* of a given species, which is equal to (V_e/V_o) x $\log_{10}$ (molecular weight of strand, g·mol^{-1}), was used to discriminate the molecularity of i-DNAs [51]. Fractions corresponding to higher-order and monomer species were determined by integration of their corresponding peaks.

Four dimensional UV melting and annealing experiments

UV absorbance spectra were recorded in the 220-330 nm wavelength range with a 1.0 nm bandwidth on a Uvikon XL Secomam UV-Visible double beam spectrophotometer (AQUALABO ANALYSE) equipped with a thermostatable 12-cell holder and a high-performance Julabo temperature controller (Seelbach). Samples were prepared in 40 mM cacodylate buffers. Spectra were acquired every 6.0 min for each cell in the 5-90 °C temperature range using a fixed temperature gradient of 0.2 °C/min during both heating and cooling processes. Stable dry air was constantly blown through the cell holder during whole acquiring process to minimize water condensation at low temperature. Spectra were recorded at a 1000 nm/s scanning rate and the temperature of a buffer solution in the reference cell was recorded at the same time. Cells were capped tightly to minimize the water evaporation at high temperature. Each oligonucleotide was added at 1.0 μM strand concentration. In order to minimize the error introduced by the possible subtle difference of strand concentration in different wells, sample concentration in each cell was calibrated with the Beer–Lambert law using the absorbance at 260 nm measured at the highest recorded temperature (i-DNAs were completely unfolded at a such high temperature) and the molar extinction coefficient of the oligonucleotide provided by the manufacturer.

Determination of pH-dependent $T_{1/2}$ or T_m values

Unless otherwise stated, the folded fraction (θ) was determined from the molar absorbance at 295 nm. θ varies between 0 and 1, corresponding to fully unfolded and fully folded species, respectively. By assuming that the transition equilibrium involves only two species (folded and unfolded), the mid-transition temperature ($T_{1/2}$, θ = 0.5) was fitted with a Boltzmann sigmoidal equation to determine the fraction folded as a function of temperature at a given pH. When the heating and cooling profiles are superimposable ($T_{1/2,\ \text{heating}} \approx T_{1/2,\ \text{cooling}}$), the folding and unfolding process are reversible, and the melting temperature (T_m) is equal to $T_{1/2}$ from either heating or cooling process. When a hysteresis between heating and cooling profiles is present ($T_{1/2,\ \text{heating}} \neq T_{1/2,\ \text{cooling}}$), both folding and unfolding process are relatively slow, and we used the average value between $T_{1/2}$ from heating and cooling processes as an approximation for the equilibrium melting temperature, T_m [53-54, 85]. This averaging method actually gives an excellent estimate of the real T_m, as illustrated in the reference [10].

Determination of temperature-dependent pH_T

From absorbances at different pHs (5.0-8.0 range) and temperatures (5.0-90.0 °C range), one can extract the pH-dependent formation fraction at a specific temperature. The pH of mid-transition (pH_T, θ = 0.5) was determined using a Boltzmann sigmoidal equation to fit the plot of formation fraction as a function of pH in the 5.0-8.0 range at a specific temperature. When the heating and cooling profiles were superimposable ($pH_{T,\text{ heating}} \approx pH_{T,\text{ cooling}}$), the averaged pH_T is equal to the pH_T from either heating or cooling process; when a hysteresis between is present ($pH_{T,\text{ heating}} \neq pH_{T,\text{ cooling}}$), the averaged pH_T is equal to the average value of pH_T from heating and cooling processes.

Circular dichroism measurements

Experiments were conducted on a J-1500 CD spectrophotometer (JASCO) in the 220-330 nm wavelength range with a 1.0 nm bandwidth at 20 °C. The samples used for UV absorbance were used. The corresponding buffer scan was subtracted from each sample scan before data processing. CD profiles were also calibrated by the measured DNA concentration. The signal changes at 288 nm for CD ellipticity were used to calculate pH_T of the structure switching from a stable i-DNA to a random coil, and pH_T was obtained by fitting the signals versus pH values with a Boltzmann sigmoidal function.

ASSOCIATED CONTENT

This Supporting Information is available free of charge via the internet at http://pubs.acs.org/XXX", including **Figures S1-S19**, and **Tables S1-S8**.

AUTHOR INFORMATION

Corresponding Authors

*Mingpan Cheng (m821315457@outlook.com);

*Jun Zhou (jun.zhou@nju.edu.cn);

*Jean-Louis Mergny (jean-louis.mergny@inserm.fr).

ORCID

Mingpan Cheng: orcid.org/0000-0003-1282-0076

Jielin Chen: orcid.org/0000-0003-4930-2870

Huangxian Ju: orcid.org/0000-0002-6741-5302

Jun Zhou: orcid.org/0000-0002-6793-3169

Jean-Louis Mergny: orcid.org/0000-0003-3043-8401

Notes

The authors declare no competing financial interest.

ACKNOWLEDGMENTS

M.C. benefited from a post-doctoral fellowship from Idex Bordeaux. J.Z. acknowledges support from the National Natural Science Foundation of China (21977045), Fundamental Research Funds for the Central Universities (02051430210). J.L.M. acknowledges the funds of Nanjing University (020514912216). This work was also supported by the China Postdoctoral Science Foundation (2019M661793).

REFERENCES

1. Gehring, K.; Leroy, J.-L.; Guéron, M., A tetrameric DNA structure with protonated cytosine·cytosine base pairs. *Nature* **1993,** *363* (6429), 561-565.
2. Kang, C. H.; Berger, I.; Lockshin, C.; Ratliff, R.; Moyzis, R.; Rich, A., Crystal structure of intercalated four-stranded d(C_3T) at 1.4 A resolution. *Proc. Natl. Acad. Sci. U. S. A.* **1994,** *91* (24), 11636-11640.
3. Marsh, R. E.; Bierstedt, R.; Eichhorn, E. L., The crystal structure of cytosine-5-acetic acid. *Acta Cryst.* **1962,** *15* (4), 310-316.
4. Langridge, R.; Rich, A., Molecular structure of helical polycytidylic acid. *Nature* **1963,** *198*, 725-728.
5. Mergny, J.-L.; Lacroix, L.; Han, X.; Leroy, J.-L.; Hélène, C., Intramolecular folding of pyrimidine oligodeoxynucleotides into an i-DNA motif. *J. Am. Chem. Soc.* **1995,** *117* (35), 8887-8898.
6. Han, X.; Leroy, J.-L.; Guéron, M., An intramolecular i-motif: the solution structure and base-pair opening kinetics of d(5m$CCT_3CCT_3ACCT_3$CC). *J. Mol. Biol.* **1998,** *278* (5), 949-965.
7. Phan, A. T.; Guéron, M.; Leroy, J.-L., The solution structure and internal motions of a fragment of the cytidine-rich strand of the human telomere. *J. Mol. Biol.* **2000,** *299* (1), 123-144.
8. Nonin-Lecomte, S.; Leroy, J.-L., Structure of a C-rich strand fragment of the human centromeric satellite III: a pH-dependent intercalation topology. *J. Mol. Biol.* **2001,** *309* (2), 491-506.
9. Leroy, J.-L.; Guéron, M.; Mergny, J.-L.; Hélène, C., Intramolecular folding of a fragment of the cytosine-rich strand of telomeric DNA into an i-motif. *Nucleic Acids Res.* **1994,** *22* (9), 1600-1606.
10. Mergny, J.-L.; Lacroix, L., Kinetics and thermodynamics of i-DNA formation: phosphodiester versus modified oligodeoxynucleotides. *Nucleic Acids Res.* **1998,** *26* (21), 4797-4803.
11. Školáková, P.; Renčiuk, D.; Palacký, J.; Krafčík, D.; Dvořáková, Z.; Kejnovská, I.; Bednářová, K.; Vorlíčková, M., Systematic investigation of sequence requirements for DNA i-motif formation. *Nucleic Acids Res.* **2019,** *47* (5), 2177-2189.
12. Rogers, R. A.; Fleming, A. M.; Burrows, C. J., Unusual isothermal hysteresis in DNA i-motif pH transitions: a study of the RAD17 promoter sequence. *Biophys. J.* **2018,** *114* (8), 1804-1815.
13. Wright, E. P.; Huppert, J. L.; Waller, Z. A. E., Identification of multiple genomic DNA sequences which form i-motif structures at neutral pH. *Nucleic Acids Res.* **2017,** *45* (6), 2951-2959.
14. Mir, B.; Serrano, I.; Buitrago, D.; Orozco, M.; Escaja, N.; Gonzalez, C., Prevalent sequences in the human genome can form mini i-motif structures at physiological pH. *J. Am. Chem. Soc.* **2017,** *139* (40), 13985-13988.
15. Fleming, A. M.; Ding, Y.; Rogers, R. A.; Zhu, J.; Zhu, J.; Burton, A. D.; Carlisle, C. B.; Burrows, C. J., 4n-1 is a "sweet spot" in DNA i-motif folding of 2'-deoxycytidine homopolymers. *J. Am. Chem. Soc.* **2017,** *139* (13), 4682-4689.
16. Nesterova, I. V.; Nesterov, E. E., Rational design of highly responsive pH sensors based on DNA i-motif. *J. Am. Chem. Soc.* **2014,** *136* (25), 8843-8846.
17. Choi, J.; Kim, S.; Tachikawa, T.; Fujitsuka, M.; Majima, T., pH-induced intramolecular folding dynamics of i-motif DNA. *J. Am. Chem. Soc.* **2011,** *133* (40), 16146-16153.
18. Zhao, Y.; Zeng, Z. X.; Kan, Z. Y.; Hao, Y. H.; Tan, Z., The folding and unfolding kinetics of the i-motif structure formed by the C-rich strand of human telomere DNA. *ChemBioChem* **2005,** *6* (11), 1957-1960.
19. Canalia, M.; Leroy, J.-L., Structure, internal motions and association-dissociation kinetics of the i-motif dimer of d(5mCCTCACTCC). *Nucleic Acids Res.* **2005,** *33* (17), 5471-5481.
20. Cheng, M.; Qiu, D.; Tamon, L.; Ištvánková, E.; Víšková, P.; Amrane, S.; Guédin, A.; Chen, J.; Lacroix, L.; Ju, H.; Trantírek, L.; Sahakyan, A. B.; Zhou, J.; Mergny, J.-L., Thermal and pH stabilities of i-DNA: Confronting in vitro experiments with models and in-cell NMR data. *Angew. Chem., Int. Ed.* **2021**, doi: 10.1002/anie.202016801.
21. Abdelhamid, M. A. S.; Waller, Z. A. E., Tricky topology: persistence of folded human telomeric i-motif DNA at ambient temperature and neutral pH. *Front. Chem.* **2020,** *8*, 40.
22. Brazier, J. A.; Shah, A.; Brown, G. D., I-motif formation in gene promoters: unusually stable formation in sequences complementary to known G-quadruplexes. *Chem. Commun.* **2012,** *48* (87), 10739-10741.
23. Kendrick, S.; Akiyama, Y.; Hecht, S. M.; Hurley, L. H., The i-motif in the *bcl-2* P1 promoter forms an unexpectedly stable structure with a unique 8:5:7 loop folding pattern. *J. Am. Chem. Soc.* **2009,** *131* (48), 17667-17676.
24. Iaccarino, N.; Cheng, M.; Qiu, D.; Pagano, B.; Amato, J.; Porzio, A. D.; Zhou, J.; Randazzo, A.; Mergny, J.-L., Effects of sequence and base composition on the CD and TDS profiles of i-DNA. *Angew. Chem., Int. Ed.* **2021**, doi: 10.1002/anie.202016822.
25. Li, X.; Peng, Y.; Ren, J.; Qu, X., Carboxyl-modified single-walled carbon nanotubes selectively induce human telomeric i-motif formation. *Proc. Natl. Acad. Sci. U. S. A.* **2006,** *103* (52), 19658-19663.
26. Chen, Y.; Qu, K.; Zhao, C.; Wu, L.; Ren, J.; Wang, J.; Qu, X., Insights into the biomedical effects of carboxylated single-wall carbon nanotubes on telomerase and telomeres. *Nat. Commun.* **2012,** *3*, 1074.
27. Dzatko, S.; Krafcikova, M.; Hansel-Hertsch, R.; Fessl, T.; Fiala, R.; Loja, T.; Krafcik, D.; Mergny, J.-L.; Foldynova-Trantirkova, S.; Trantirek, L., Evaluation of the stability of DNA i-motifs in the nuclei of living mammalian cells. *Angew. Chem., Int. Ed.* **2018,** *57* (8), 2165-2169.
28. Zeraati, M.; Langley, D. B.; Schofield, P.; Moye, A. L.; Rouet, R.; Hughes, W. E.; Bryan, T. M.; Dinger, M. E.; Christ, D., I-motif DNA structures are formed in the nuclei of human cells. *Nat. Chem.* **2018,** *10* (6), 631-637.

29. Leroy, J.-L.; Guéron, M., Solution structures of the i-motif tetramers of d(TCC), d(5methylCCT) and d(T5methylCC): novel NOE connections between amino protons and sugar protons. *Structure* **1995,** *3* (1), 101-120.
30. Cai, L.; Chen, L.; Raghavan, S.; Ratliff, R.; Moyzis, R.; Rich, A., Intercalated cytosine motif and novel adenine clusters in the crystal structure of the *Tetrahymena* telomere. *Nucleic Acids Res.* **1998,** *26* (20), 4696-4705.
31. Snoussi, K.; Nonin-Lecomte, S.; Leroy, J.-L., The RNA i-motif. *J. Mol. Biol.* **2001,** *309* (1), 139-153.
32. Esmaili, N.; Leroy, J.-L., i-motif solution structure and dynamics of the d(AACCCC) and d(CCCCAA) tetrahymena telomeric repeats. *Nucleic Acids Res.* **2005,** *33* (1), 213-224.
33. Lieblein, A. L.; Buck, J.; Schlepckow, K.; Fürtig, B.; Schwalbe, H., Time-resolved NMR spectroscopic studies of DNA i-motif folding reveal kinetic partitioning. *Angew. Chem., Int. Ed.* **2012,** *51* (1), 250-253.
34. Lieblein, A. L.; Fürtig, B.; Schwalbe, H., Optimizing the kinetics and thermodynamics of DNA i-motif folding. *ChemBioChem* **2013,** *14* (10), 1226-1230.
35. Fleming, A. M.; Stewart, K. M.; Eyring, G. M.; Ball, T. E.; Burrows, C. J., Unraveling the 4n - 1 rule for DNA i-motif stability: base pairs vs. loop lengths. *Org. Biomol. Chem.* **2018,** *16* (24), 4537-4546.
36. Liu, L.; Kim, B. G.; Feroze, U.; Macgregor, R. B., Jr.; Chalikian, T. V., Probing the ionic atmosphere and hydration of the c-MYC i-motif. *J. Am. Chem. Soc.* **2018,** *140* (6), 2229-2238.
37. Chu, B.; Zhang, D.; Paukstelis, P. J., A DNA G-quadruplex/i-motif hybrid. *Nucleic Acids Res.* **2019,** *47* (22), 11921-11930.
38. Iaccarino, N.; Di Porzio, A.; Amato, J.; Pagano, B.; Brancaccio, D.; Novellino, E.; Leardi, R.; Randazzo, A., Assessing the influence of pH and cationic strength on i-motif DNA structure. *Anal. Bioanal. Chem.* **2019,** *411* (28), 7473-7479.
39. Volker, J.; Klump, H. H.; Breslauer, K. J., The energetics of i-DNA tetraplex structures formed intermolecularly by d(TC_5) and intramolecularly by d[$(C_5T_3)_3C_5$]. *Biopolymers* **2007,** *86* (2), 136-147.
40. Day, H. A.; Wright, E. P.; MacDonald, C. J.; Gates, A. J.; Waller, Z. A. E., Reversible DNA i-motif to hairpin switching induced by copper(II) cations. *Chem. Commun.* **2015,** *51* (74), 14099-14102.
41. Day, H. A.; Huguin, C.; Waller, Z. A. E., Silver cations fold i-motif at neutral pH. *Chem. Commun.* **2013,** *49* (70), 7696-7698.
42. Kohagen, M.; Uhlig, F.; Smiatek, J., On the nature of ion‐stabilized cytosine pairs in DNA i‐motifs: the importance of charge transfer processes. *Int. J. Quantum Chem.* **2019,** *119* (14), e25933.
43. Abdelhamid, M. A.; Fabian, L.; MacDonald, C. J.; Cheesman, M. R.; Gates, A. J.; Waller, Z. A. E., Redox-dependent control of i-motif DNA structure using copper cations. *Nucleic Acids Res.* **2018,** *46* (12), 5886-5893.
44. Gao, J.; Berden, G.; Rodgers, M. T.; Oomens, J., Interaction of Cu^+ with cytosine and formation of i-motif-like C-M^+-C complexes: alkali versus coinage metals. *Phys. Chem. Chem. Phys.* **2016,** *18* (10), 7269-7277.
45. Miyoshi, D.; Matsumura, S.; Nakano, S.; Sugimoto, N., Duplex dissociation of telomere DNAs induced by molecular crowding. *J. Am. Chem. Soc.* **2004,** *126* (1), 165-169.
46. Rajendran, A.; Nakano, S.; Sugimoto, N., Molecular crowding of the cosolutes induces an intramolecular i-motif structure of triplet repeat DNA oligomers at neutral pH. *Chem. Commun.* **2010,** *46* (8), 1299-1301.
47. Paul, S.; Hossain, S. S.; Samanta, A., Insights into the folding pathway of a c-MYC-promoter-based i-motif DNA in crowded environments at the single-molecule level. *J. Phys. Chem. B* **2020,** *124* (5), 763-770.
48. Reilly, S. M.; Morgan, R. K.; Brooks, T. A.; Wadkins, R. M., Effect of interior loop length on the thermal stability and p*K*a of i-motif DNA. *Biochemistry* **2015,** *54* (6), 1364-1370.
49. Bhavsar-Jog, Y. P.; Van Dornshuld, E.; Brooks, T. A.; Tschumper, G. S.; Wadkins, R. M., Epigenetic modification, dehydration, and molecular crowding effects on the thermodynamics of i-motif structure formation from C-rich DNA. *Biochemistry* **2014,** *53* (10), 1586-1594.
50. Cui, J.; Waltman, P.; Le, V. H.; Lewis, E. A., The effect of molecular crowding on the stability of human c-MYC promoter sequence i-motif at neutral pH. *Molecules* **2013,** *18* (10), 12751-12767.
51. Largy, E.; Mergny, J.-L., Shape matters: size-exclusion HPLC for the study of nucleic acid structural polymorphism. *Nucleic Acids Res.* **2014,** *42* (19), e149.
52. Dailey, M. M.; Miller, M. C.; Bates, P. J.; Lane, A. N.; Trent, J. O., Resolution and characterization of the structural polymorphism of a single quadruplex-forming sequence. *Nucleic Acids Res.* **2010,** *38* (14), 4877-4888.
53. Mergny, J.-L.; Li, J.; Lacroix, L.; Amrane, S.; Chaires, J. B., Thermal difference spectra: a specific signature for nucleic acid structures. *Nucleic Acids Res.* **2005,** *33* (16), e138.
54. Mergny, J.-L.; Lacroix, L., Analysis of thermal melting curves. *Oligonucleotides* **2003,** *13* (6), 515-537.
55. Kaiser, C. E.; Van Ert, N. A.; Agrawal, P.; Chawla, R.; Yang, D.; Hurley, L. H., Insight into the complexity of the i-motif and G-quadruplex DNA structures formed in the KRAS promoter and subsequent drug-induced gene repression. *J. Am. Chem. Soc.* **2017,** *139* (25), 8522-8536.
56. Kang, H. J.; Kendrick, S.; Hecht, S. M.; Hurley, L. H., The transcriptional complex between the *BCL2* i-motif and hnRNP LL is a molecular switch for control of gene expression that can be modulated by small molecules. *J. Am. Chem. Soc.* **2014,** *136* (11), 4172-4185.
57. Abou Assi, H.; Garavis, M.; Gonzalez, C.; Damha, M. J., i-Motif DNA: structural features and significance to cell biology. *Nucleic Acids Res.* **2018,** *46* (16), 8038-8056.
58. Takahashi, S.; Sugimoto, N., Stability prediction of canonical and non-canonical structures of nucleic acids in various molecular environments and cells. *Chem. Soc. Rev.* **2020,** *49* (23), 8439-8468.

59. SantaLucia, J., Jr.; Allawi, H. T.; Seneviratne, P. A., Improved nearest-neighbor parameters for predicting DNA duplex stability. *Biochemistry* **1996,** *35* (11), 3555-3562.
60. Panjkovich, A.; Melo, F., Comparison of different melting temperature calculation methods for short DNA sequences. *Bioinformatics* **2005,** *21* (6), 711-722.
61. Rogers, R. A.; Meyer, M. R.; Stewart, K. M.; Eyring, G. M.; Fleming, A. M.; Burrows, C. J., Hysteresis in poly-2'-deoxycytidine i-motif folding is impacted by the method of analysis as well as loop and stem lengths. *Biopolymers* **2021,** *112* (1), e23389.
62. Chen, L.; Cai, L.; Zhang, X.; Rich, A., Crystal structure of a four-stranded intercalated DNA: d(C4). *Biochemistry* **1994,** *33* (46), 13540-13546.
63. Leroy, J.-L., T·T pair intercalation and duplex interconversion within i-motif tetramers. *J. Mol. Biol.* **2003,** *333* (1), 125-139.
64. Leroy, J.-L.; Snoussi, K.; Gureon, M., Investigation of the energetics of C–H···O hydrogen bonds in the DNA i-motifvia the equilibrium between alternative intercalation topologies. *Magn. Reson. Chem.* **2001,** *39* (S1), S171-S176.
65. Canalia, M.; Leroy, J.-L., $[5mCCTCTCTCC]_4$: an i-motif tetramer with intercalated T•T pairs. *J. Am. Chem. Soc.* **2009,** *131* (36), 12870-12871.
66. Berger, I.; Egli, M.; Rich, A., Inter-strand C-H···O hydrogen bonds stabilizing four-stranded intercalated molecules: stereoelectronic effects of O4' in cytosine-rich DNA. *Proc. Natl. Acad. Sci. U. S. A.* **1996,** *93* (22), 12116-12121.
67. Owczarzy, R.; Moreira, B. G.; You, Y.; Behlke, M. A.; Walder, J. A., Predicting stability of DNA duplexes in solutions containing magnesium and monovalent cations. *Biochemistry* **2008,** *47* (19), 5336-5353.
68. Shkel, I. A.; Knowles, D. B.; Record, M. T., Jr., Separating chemical and excluded volume interactions of polyethylene glycols with native proteins: comparison with PEG effects on DNA helix formation. *Biopolymers* **2015,** *103* (9), 517-527.
69. Buscaglia, R.; Miller, M. C.; Dean, W. L.; Gray, R. D.; Lane, A. N.; Trent, J. O.; Chaires, J. B., Polyethylene glycol binding alters human telomere G-quadruplex structure by conformational selection. *Nucleic Acids Res.* **2013,** *41* (16), 7934-7946.
70. Hänsel, R.; Löhr, F.; Foldynová-Trantírková, S.; Bamberg, E.; Trantírek, L.; Dötsch, V., The parallel G-quadruplex structure of vertebrate telomeric repeat sequences is not the preferred folding topology under physiological conditions. *Nucleic Acids Res.* **2011,** *39* (13), 5768-5775.
71. Niu, K.; Zhang, X.; Deng, H.; Wu, F.; Ren, Y.; Xiang, H.; Zheng, S.; Liu, L.; Huang, L.; Zeng, B.; Li, S.; Xia, Q.; Song, Q.; Palli, S. R.; Feng, Q., BmILF and i-motif structure are involved in transcriptional regulation of *BmPOUM2* in *Bombyx mori*. *Nucleic Acids Res.* **2018,** *46* (4), 1710-1723.
72. Lacroix, L.; Lienard, H.; Labourier, E.; Djavaheri-Mergny, M.; Lacoste, J.; Leffers, H.; Tazi, J.; Helene, C.; Mergny, J.-L., Identification of two human nuclear proteins that recognise the cytosine-rich strand of human telomeres *in vitro*. *Nucleic Acids Res.* **2000,** *28* (7), 1564-1575.
73. Marsich, E.; Xodo, L. E.; Manzini, G., Widespread presence in mammals and high binding specificity of a nuclear protein that recognises the single-stranded telomeric motif $(CCCTAA)_n$. *Eur. J. Biochem.* **1998,** *258* (1), 93-99.
74. Marsich, E.; Piccini, A.; Xodo, L. E.; Manzini, G., Evidence for a HeLa nuclear protein that binds specifically to the single-stranded d(CCCTAA)n telomeric motif. *Nucleic Acids Res.* **1996,** *24* (20), 4029-4033.
75. Webb, B. A.; Chimenti, M.; Jacobson, M. P.; Barber, D. L., Dysregulated pH: a perfect storm for cancer progression. *Nat. Rev. Cancer* **2011,** *11* (9), 671-677.
76. Gadsby, D. C., Ion channels versus ion pumps: the principal difference, in principle. *Nat. Rev. Mol. Cell Biol.* **2009,** *10* (5), 344-352.
77. Litan, A.; Langhans, S. A., Cancer as a channelopathy: ion channels and pumps in tumor development and progression. *Front. Cell. Neurosci.* **2015,** *9*, 86.
78. Warner, D. A.; Shine, R., The adaptive significance of temperature-dependent sex determination in a reptile. *Nature* **2008,** *451* (7178), 566-568.
79. Patel, D.; Franklin, K. A., Temperature-regulation of plant architecture. *Plant Signaling Behav.* **2009,** *4* (7), 577-579.
80. Protsiv, M.; Ley, C.; Lankester, J.; Hastie, T.; Parsonnet, J., Decreasing human body temperature in the United States since the industrial revolution. *eLife* **2020,** *9*, e49555.
81. Casey, J. R.; Grinstein, S.; Orlowski, J., Sensors and regulators of intracellular pH. *Nat. Rev. Mol. Cell Biol.* **2010,** *11* (1), 50-61.
82. Leung, K.; Chakraborty, K.; Saminathan, A.; Krishnan, Y., A DNA nanomachine chemically resolves lysosomes in live cells. *Nat. Nanotechnol.* **2019,** *14* (2), 176-183.
83. Mergny, J.-L.; Sen, D., DNA quadruple helices in nanotechnology. *Chem. Rev.* **2019,** *119* (10), 6290-6325.
84. Debnath, M.; Fatma, K.; Dash, J., Chemical regulation of DNA i-motifs for nanobiotechnology and therapeutics. *Angew. Chem., Int. Ed.* **2019,** *58* (10), 2942-2957.
85. Mergny, J.-L.; Lacroix, L., UV melting of G-quadruplexes. *Curr. Protoc. Nucleic Acid Chem.* **2009,** *Chapter 17*, Unit 17.1.

Table of Contents (TOC)

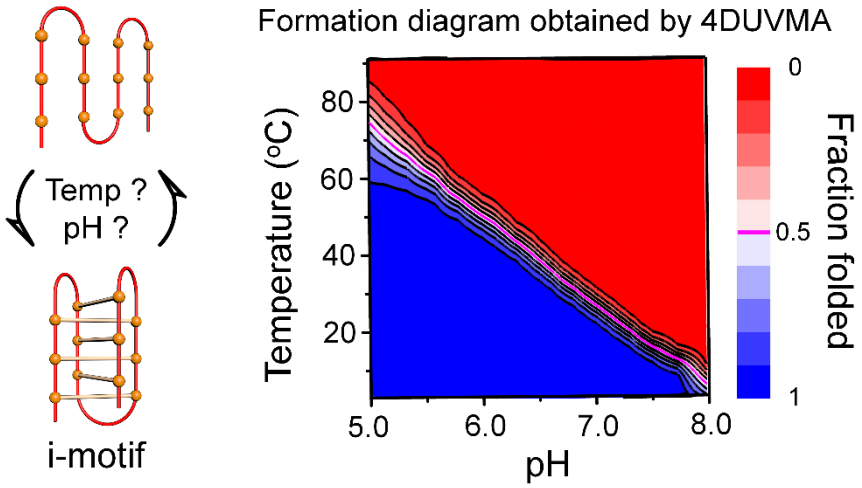

A method called 4DUVMA was developed to analyze i-motif formation under a variety of pH and temperature combinations.